Sol-gel processing of a covalent organic framework for the generation of hierarchically porous monolithic adsorbents

*Mark E. Carrington[a,‡], Nakul Rampal[a,‡], David G. Madden[a], Daniel O'Nolan[b], Nicola Pietro Maria Casati[c], Giorgio Divitini[d], Ritums Cepitis[e], Jesús Á. Martín-Illán[f], Ceren Çamur[a], Joaquin Silvestre-Albero[g], Felix Zamora[f], Sergei Taraskin[e], Karena Chapman[b], David Fairen-Jimenez[a *]*

[a]*The Adsorption & Advanced Materials Laboratory (AAML), Department of Chemical Engineering & Biotechnology, University of Cambridge, Philippa Fawcett Drive, Cambridge CB3 0AS, UK.*

[b]*Department of Chemistry, Stony Brook University, 100 Nicholls Road, Stony Brook, New York 11794, United States.*

[c]*Laboratory for Synchrotron Radiation—Condensed Matter, Paul Scherrer Institute, 5232 Villigen–PSI, Switzerland.*

[d] *Electron Microscopy Group, Department of Materials Science and Metallurgy, University of Cambridge, 27 Charles Babbage Road, Cambridge CB3 0FS, U.K.*

[e] *Department of Chemistry, University of Cambridge, Lensfield Road, Cambridge CB2 1EW, U.K.*

[f]*Departamento de Química Inorgánica, Universidad Autónoma de Madrid, 28049 Madrid, Spain.*

[g] *Laboratorio de Materiales Avanzados, Dpto. de Química Inorgánica-Instituto Universitario de Materiales, Universidad de Alicante, E-03690, San Vicente del Raspeig, Spain.*

[*]*E-mail: df334@cam.ac.uk*

[‡]These authors contributed equally

ABSTRACT. Covalent organic frameworks (COFs) have emerged as a versatile materials platform for applications including chemical separations, water purification, chemical reaction engineering and energy storage. Their inherently low mechanical stability, however, frequently renders existing methods of pelletisation ineffective contributing to pore collapse, pore blockage or insufficient densification of crystallites. Here, we present a general process for the shaping and densifying of COFs into centimetre-scale porous monolithic pellets without the need for templates, additives or binders. This process minimises mechanical damage from shear-induced plastic deformation and further provides a network of interparticle mesopores that we exploit in accessing analyte capacities above those achievable from the intrinsic porosity of the COF framework. Using a lattice-gas model, we accurately capture the monolithic structure across the mesoporous range and tie pore architecture to performance characteristics in both gas storage and separation applications. Collectively, these findings represent a substantial step in the practical applicability of COFs and other mechanically weak porous materials.

1. Main

Porous materials capable of reducing both the cost and energy intensity of industrial chemical processes are critically needed in transitioning to a carbon-neutral energy cycle.[1, 2] Constructed from earth-abundant elements and affording a combination of chemo-structural diversity, ease of synthetic modification and relative chemical stability, covalent organic frameworks (COFs) have emerged as attractive alternatives to existing porous materials including activated carbons, zeolites and metal–organic frameworks (MOFs).[3-5] However, a technological limit has been reached where traditional methods of adsorbent post-processing are poorly suited to COFs as a result of the low mechanical stability frequently exhibited by these materials.[6-11] To date, these mechanical characteristics have been shown to limit the pressures that can be used during pelletisation[10, 12] and the selection of fluids available for activation[6-8] – deviations from which can result in sharp losses in capacity. While factors such as framework topology and linker length can be synthetically tuned to target more robust architectures[13], the inverse approach has not been attempted – i.e., whereby a desired COF can be shaped into an industrially relevant form factor without compromising key performance metrics.

Here, we report a rapid and general process for the shaping of COFs into macroscopic pellets without the use of binders, templates or additives, and without any further processing steps needed for a final application. For an archetypical two-dimensional (2D) COF, TPB-DMTP-COF,[14] we demonstrate control over the degree of aggregation of crystallites within pellets and systematically identify the presence of a lower limit in inter-crystallite pore size for a given activation solvent. We tie this limit to the onset of capillary-action induced, turbostratic disordering of crystallites and further confirm that mechanical damage can be avoided through the use of an ultra-low surface tension activation fluid. COF monoliths thus prepared exhibit identical low-pressure adsorption characteristics to those of the best-reported powder analogues and, additionally, benefit from a system of interparticle mesopores that push final adsorption capacities above levels expected for single crystals. We capture these structural characteristics in a lattice-gas model, which accurately reproduces experimentally-derived isotherms for COF monoliths *in silico*. The combination of intact crystallites and hierarchical mesopores in an industrially-suitable pellet endows COF monoliths with superior adsorption properties relative to powders, which we demonstrate for both pure component gas storage (CO_2 and CH_4) and mixed gas chemical separation (CO_2/N_2 and CO_2/CH_4) applications. Based on these findings, our work not only provides a path forward for the industrial applicability of COFs but a systematic framework through which COF microstructure and final adsorption properties can be tuned without altering the underlying COF chemistry.

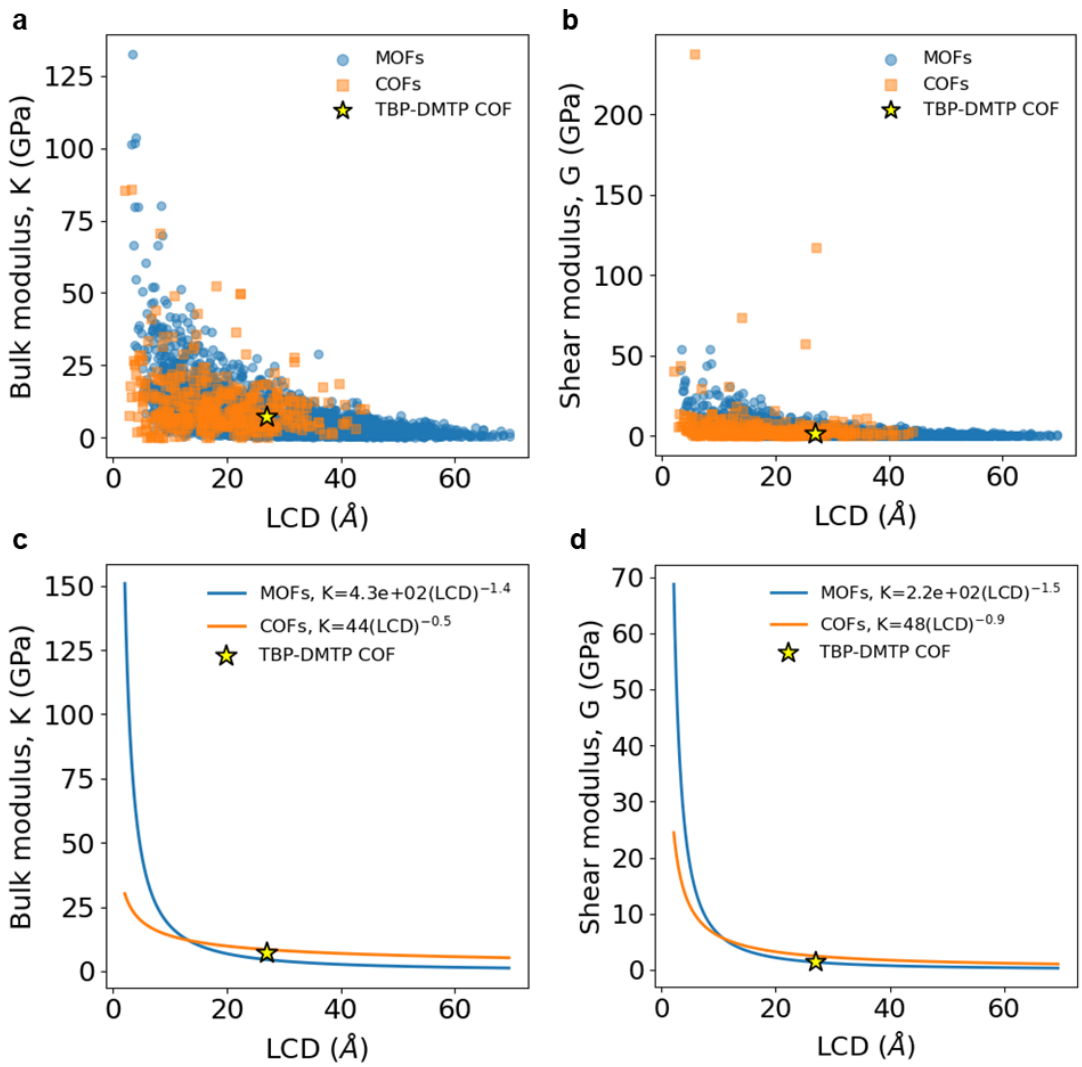

Figure 1 | Mechanical properties calculation. **(a)** Relationship between bulk modulus, K (GPa), and LCD (Å) and **(b)** between shear modulus, G (GPa), and LCD (Å) with MOFs in blue (circle), COFs in orange (square), and TPB-DMTP-COF in yellow (star). **(c, d)** Exponential fits to the data shown in figures (a) and (b), respectively, with MOFs in blue, COFs in orange, and TPB-DMTP COF in yellow (star).

2. High-throughput mechanical properties calculation

2D COFs are thought to be unstable to in-plane mechanical shear.[9] To evaluate the mechanical properties of COFs across topologies and linkage chemistries, we first performed a high-throughput screen of all reported COFs as inventoried in the CURATED-COF database[15] and compared their bulk moduli, shear moduli and elastic constants to those of MOFs[13] (**Figure 1**). Within a largest cavity diameter (LCD) range of 15-40 Å, the bulk and shear moduli of COFs were found to be similar to those of MOFs, with COFs exhibiting marginally higher bulk moduli and shear moduli on average. However, at lower LCD ranges characteristic of ultramicroporous (< 7 Å) and microporous (< 20 Å) materials, the bulk and shear moduli of COFs were found to be substantially lower than those of MOFs, suggesting an inherently greater tendency of COFs to mechanically deform even in the absence of larger (> 15 Å) pores. To gain insights into the mechanical stability of these materials, we

then analysed the elastic constants of a representative COF subset, hexagonal 2D COFs, which currently account for 54% of 2D COFs and 45% of all COFs synthesised to date. Applying the stability criteria: $c_{11} > |c_{12}|$, $c_{33}(c_{11} + 2c_{12}) > 2(c_{13})^2$, $c_{11}c_{33} > (c_{13})^2$ and $c_{44} > 0$, a majority (64%) of hexagonal 2D COFs were found to be unstable, confirming weakness to mechanical shear as a predominating feature of these materials and possibly shedding light on the low degrees of crystallinity frequently exhibited by these materials. As conventional methods of powder pelletization routinely employ pressures in the range of 1-3 GPa, which are known to trigger losses in capacity within MOFs,[16-20] a revised approach for COF processing and pelletisation was sought.

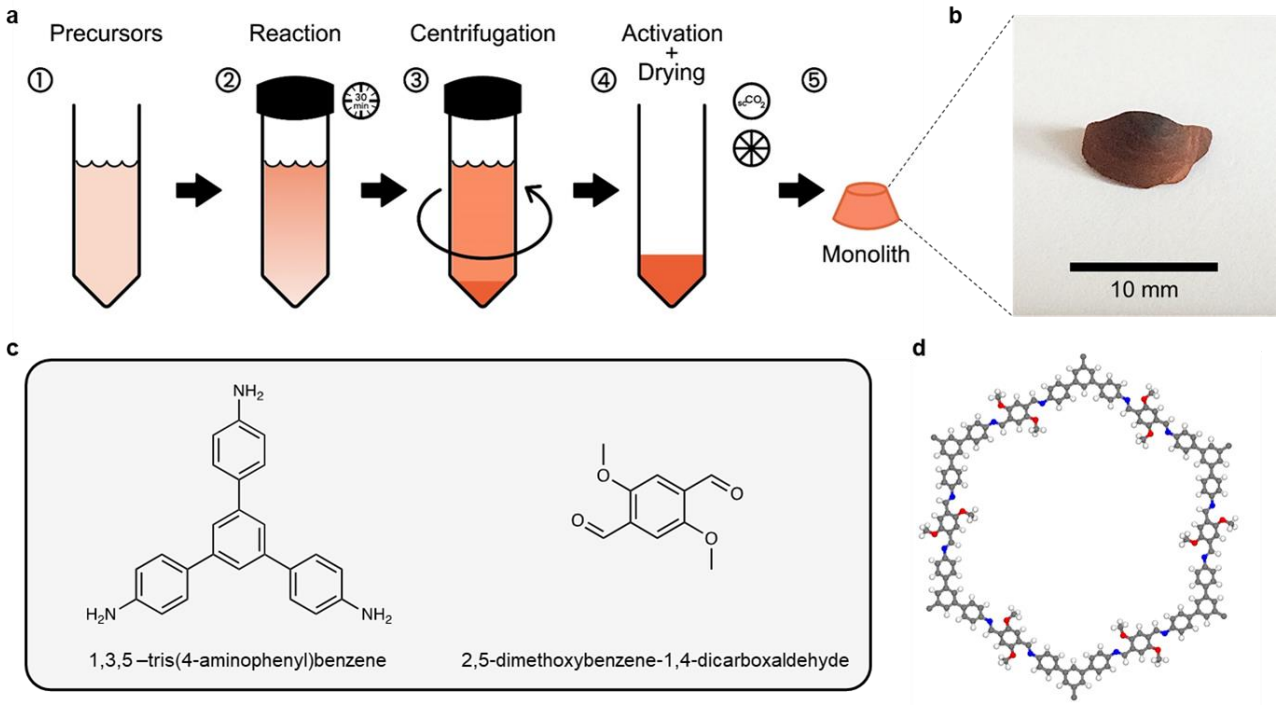

Figure 2 | TPB-DMTP-COF monolith synthesis and structure. **(a)** Processing workflow for TPB-DMTP-COF monolith formation. **(b)** TPB-DMTP-COF monolith. **(c)** Organic precursors used in the synthesis of the COF monolith. **(d)** Pore structure of TPB-DMTP-COF with C atoms in grey, N atoms in blue, O atoms in red, and H atoms in white.

3. Sol-gel synthesis of COFs

To permit ease of experimental benchmarking and analysis, TPB-DMTP-COF was identified as a representative 2D COF with an LCD of 25 Å and excellent known crystallinity. Upon screening a variety of synthesis solvent systems, acetonitrile and a 1:1 (v/v) mixture of 1,3,5-trimethylbenzene (mesitylene) and 1,4-dioxane (dioxane) were identified as two systems capable of both solubilising the starting materials and producing crystalline samples of TPB-DMTP-COF. However, whereas the 1:1 (v/v) mixture of mesitylene and dioxane produced powder samples consisting of aggregated particles > 500 nm in diameter (**Figure S5a**), the acetonitrile system produced dense pellets consistent with those previously described for MOF monoliths and composed of particles of *ca.* 40 nm in diameter (**Figure S5h**) – well within limits previously established for monolith formation in MOFs[17,

[18] (*i.e.* < 120 nm). Taking these two systems as extremes, solvent compositions consisting of different fractions of each were used to prepare pellets following a process workflow that consisted of: (1) reaction for a fixed amount of time (typically 30 minutes), (2) centrifugation, (3) purification and solvent exchange to methanol, and (4) controlled drying and activation **(Figure 2)**.

Upon processing, scanning electron microscopy (SEM) of the finished pellets revealed a gradual progression in microstructure from larger, loosely aggregated particles to densely packed monoliths exhibiting conchoidal fracture and little to no inter-particle free volume (**Figure S5**). Analysis of the nitrogen adsorption isotherms (**Figure S3**) collected for these pellets, however, revealed a striking trend. Whereas we observed a monotonic increase in Brunauer-Emmett-Teller (BET) area – calculated using BETSI[21] – for pellets synthesized in solvent systems containing acetonitrile fractions ranging from 0.000 – 0.750 (v/v), a sharp decrease in BET area to 4 m^2 g^{-1} was observed for samples prepared at higher acetonitrile fractions (**Figure 3c**). As a result, the highest BET area that could be obtained for TPB-DMTP-COF using methanol as the activation solvent was 1,122 m^2 g^{-1} suggesting the presence of a lower limit in inter-crystallite pore size beyond which pore disruption takes place. To test whether this pore disruption was being induced by capillary-action,[8] a further sample was prepared in a pure acetonitrile solvent system and processed as before, but was dried and activated in supercritical carbon dioxide ($scCO_2$) instead of in methanol and air. The finished pellet not only recovered full porosity but lay on the monotonic trend previously described, exhibiting a BET area of 2,125 m^2 g^{-1} – slightly above those previously described for powder analogues of TPB-DMTP-COF. When a higher rate of $scCO_2$ pressure release (8 bar h^{-1} *vs.* 3 bar h^{-1}) was used during the activation of an identically prepared 1.000 acetonitrile pellet, a reduction in BET area to 1,439 m^2 g^{-1} was observed, further suggesting that losses in BET area occur as a result of capillary-action induced damage.

To gain deeper insights into the structural changes accompanying these bulk characteristics, we used a combination of pair distribution function (PDF) and X-ray diffraction (XRD). Non-negative matrix factorisation of the PDF-XRD data revealed three independent underlying components that we attribute to non-crystalline layer COF content, residual starting material content, and multilayer (*i.e.* crystalline) COF content – components A, B and C respectively (**Figure 3e**). For methanol-activated pellets below an acetonitrile fraction of 0.75, a respective decrease and increase in components A and C were observed as the acetonitrile fraction was increased, indicating that TPB-DMTP-COF crystallinity gradually improves before the onset of mechanical damage. Above an acetonitrile fraction of 0.750 (v/v), crystallinity sharply declines, resulting in an increased content of non-crystalline layer TPB-DMTP-COF as seen from the increasing weighting of component A. When

$scCO_2$ is used during drying and activation, the multi-layer content is recovered – an observation consistent with findings from nitrogen adsorption studies and providing clear evidence for a correlation between mechanical disruption of COF crystallites during post-processing and observable gas uptake capacities as previously noted for powdered COF systems[6].

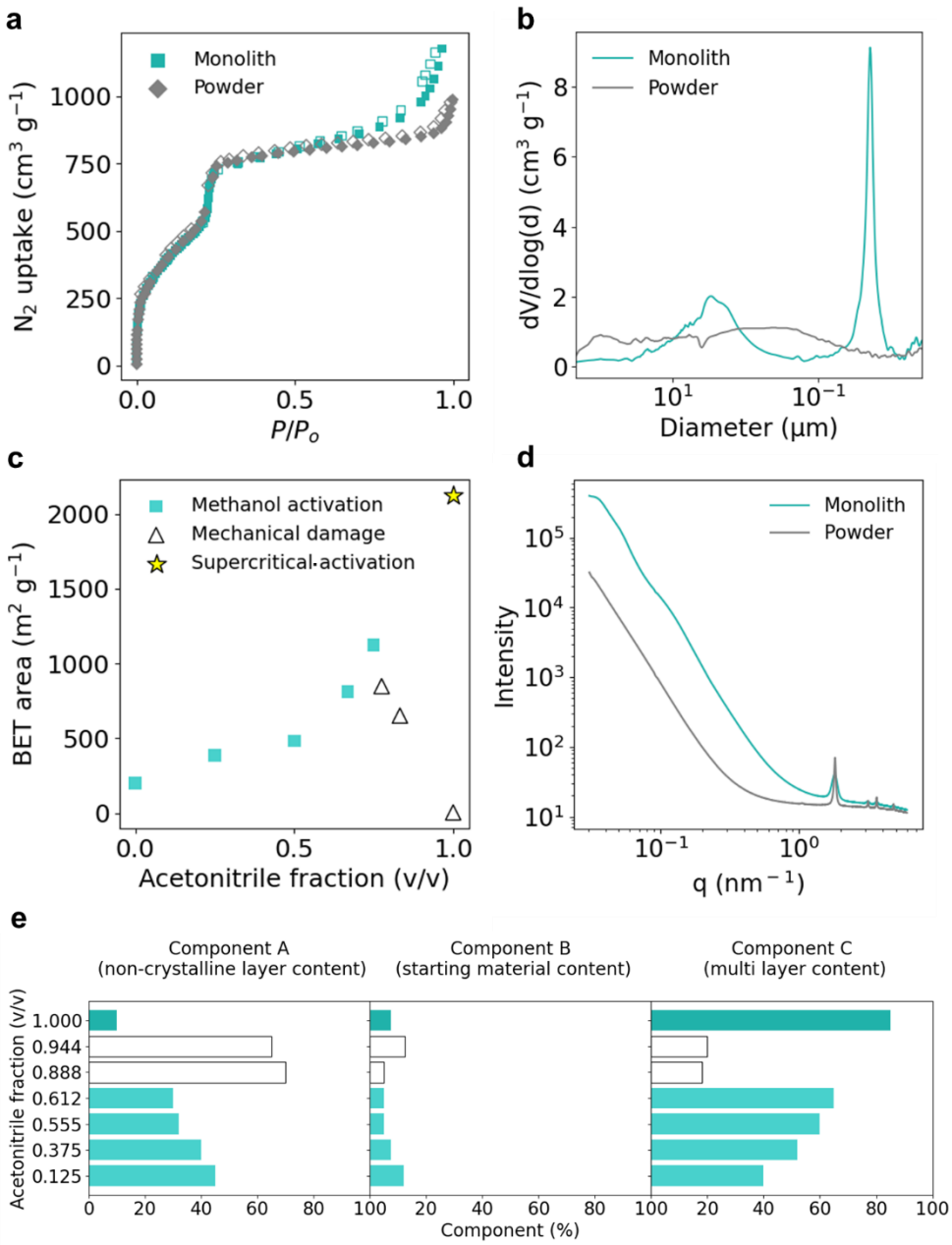

Figure 3 | Structural characteriation of TPB-DMTP-COF monoliths. **(a)** N_2 adsorption isotherms at 77 K for the 3 bar h^{-1} $scCO_2$ activated 1.000 (v/v) TPB-DMTP-COF monolith (turquoise squares), and powder (grey diamonds). **(b)** Mercury pore size distribution (PSD) of the 3 bar h^{-1} $scCO_2$ activated 1.000 (v/v) TPB-DMTP-COF monolith (turquoise), and powder (grey). **(c)** BET area *vs.* acetonitrile fraction (v/v); methanol activated samples (turquoise squares), samples with mechanical damage (white triangles), and supercritically activated (3 bar h^{-1}) sample (yellow star). **(d)** SAXS data of the supercritically activated (3 bar h^{-1}) TPB-DMTP COF monolith (turquoise), and powder (grey). **(e)** Bar chart showing the % of component A (non-crystalline layer content), component B (starting material content), and component C (multilayer content) as a function of acetonitrile fraction (v/v) for each sample studied.

To better understand the mechanism of crystallite disordering into non-crystalline layers within COF monoliths, we performed high-resolution transmission electron microscopy (HR-TEM) on a methanol-activated 1.000 acetonitrile control sample for which crystallites are sufficiently disrupted to afford a BET area of 4 m^2 g^{-1} (**Figure 4**). Analysis of the structure both within the bulk and within a few layers indicated a series of multi-layer crystalline domains bridged by turbostratic regions similar to those observed in graphitic carbon. Fourier transform analysis of the image (**Figure 4c inset**) further revealed that these features result in a single diffuse band corresponding to a real-space length of 0.36 nm – consistent with interlayer spacing values obtained from analysis of components A (0.37 nm) and C (0.35 nm) derived from the PDF-XRD data. Collectively, these findings both confirm the presence of disrupted crystallites in non-porous monoliths and suggest that a turbostratic disordering mechanism is responsible for such observable losses in porosity.

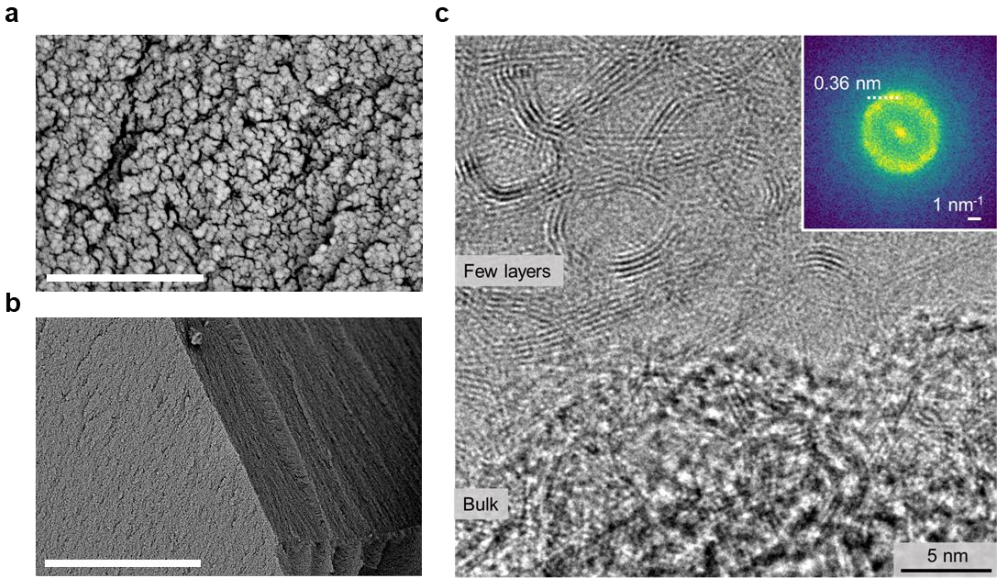

Figure 4 | SEM and TEM images of the methanol-activated 1.000 acetonitrile fraction TPB-DMTP-COF monolith (a,b) Scanning electron microscopy (SEM) images of the TPB-DMTP-COF monolith where the scale bar is 1μm for (a) and 10μm for (b). **(c)** HR-TEM image of the TPB-DMTP-COF monolith, showing locally layered structures connected by turbostratically disordered regions where the scale bar is 5 nm. The inset shows a fast fourier transform (FFT) from a thin area, indicating a broad ring, with the peak corresponding to 0.36.

With post-processing conditions capable of explicitly avoiding crystallite damage established, we then used a combination of mercury porosimetry and small-angle X-ray scattering (SAXS) to gain insights into the structure of monolith free volume elements across the mesoscale. Pore size distributions derived from mercury intrusion curves for a $scCO_2$-activated 1.000 acetonitrile pellet revealed the presence of sharp mesoporosity at 18.7 nm attributable to well-defined interparticle free volume elements (**Figure 3b**). Broader macroporosity centred at pore width of around 3 μm was also observed. By contrast, a non-monolithic powder control prepared using the method of Xu *et al.* (BET

area of 1985 m^2 g^{-1})[14] exhibited no well-defined meso- or macroporosity. Analysis of the respective mercury areas for accessible pore widths down to 3.9 nm (above that of the intrinsic framework, i.e. 2.5 nm) further showed an area of 504 m^2 g^{-1} for the monolith compared to 196 m^2 g^{-1} for the powder. These results were consistent with those derived from SAXS (**Figure 3d**). The $scCO_2$-processed monolith was well fit by a spheroidal particle model with two log normalized-distributions models with mean diameters of 25.8 nm (σ = 0.4) and 99.8 nm (σ = 0.2), indicating the presence of a mesoporous inter-particle free volume element and providing evidence for additional macroporosity. By contrast, the non-monolithic powder control was found to possess an inter-particle size distribution beyond the 0.5-100 nm range and was accordingly not fit. These results suggest that COF processing into monoliths can not only be used to avoid pore collapse but can provide additional mesoporosity, inaccessible from powders, that can be used to tune final uptake performance characteristics – potentially beyond those of purely crystalline systems.

To examine the impact of crystallite disordering on mesoporous free-volume elements, a $scCO_2$-processed monolith activated at an accelerated depressurisation rate of 8 bar h^{-1} (BET area of 1439 m^2 g^{-1}) was also analysed using SAXS (**Figure S4**). The sample was fit by three spheroidal size-distribution models exhibiting mean diameters of 14.7 nm (σ = 0.3), 21.1 nm (σ = 0.6), and 98.5 nm (σ = 0.1). The emergence of a third, narrow free volume element along with an overall shift in mesopore distribution to smaller values suggests that disruption of crystallites is concomitant with a reduction in inter-particle free volume. As this reduction in inter-particle pore size can be controlled by the $scCO_2$ pressure release rate, future opportunities exist for top-down control over monolith microstructure and gas adsorption properties.

4. Molecular simulations and lattice gas model

To accurately capture the adsorption characteristics of TPB-DMTP-COF *in silico*, we carried out grand canonical Monte Carlo (GCMC) simulations on TPB-DMTP-COF crystalline fragments exhibiting varying degrees of interlayer slip. Starting from perfect AA stacking (0% slip), one of two sequential layers of the COF was gradually shifted until perfect AB stacking was achieved (100% slip). Using cells derived from 0, 25, 40, 50, 75, and 100% slipped starting structures (**Figure S1**), GCMC simulations were then used to generate predicted nitrogen isotherms at 77 K. Upon comparison of the respective low-pressure region and mesoporous step of the experimental adsorption isotherms to those derived from theory, a 40% slipped structure was found to provide the best agreement with experiment, giving almost identical low-pressure adsorption characteristics up to the mesoporous step (**Figure 5d**). Above the mesoporous step, however, whereas experimental isotherms for TPB-DMTP-COF powders maintained a reasonable agreement with those calculated from the

40% slipped structure until saturation, substantial deviations from theory were observed for experimental isotherms derived from TPB-DMTP-COF monoliths as a result of inter-particle mesoporosity. As these deviations ultimately push total nitrogen uptake within the monolith above levels expected for purely crystalline systems, the ability to accurately capture such deviations computationally is critical in evaluating and subsequently tuning final gas uptake characteristics for a desired target application.

To model contributions to total gas uptake arising from inter-particle mesopores, we moved to a lattice gas model of the TPB-DMTP-COF monolith. Lattice gas models have been extensively used in the past to study the nature of sorption hysteresis for fluids in confined interconnected void spaces of porous glasses.[18,19] The structural model of the monolith (**Figure 5b**) used in the lattice-gas model was numerically reconstructed from the SAXS data for the TPB-DMTP-COF monolith by means of generating a two-point correlation function $S_2(r)$ and using it in the reconstruction algorithm. A 3D reconstructed structure and its 2D slice used in the lattice gas model for the TPB-DMTP-COF monolith activated using supercritical carbon dioxide are shown in **Figures 5a** and **5c** respectively. To model the trajectory of the system in the grand canonical ensemble, we subsequently employed kinetic Monte Carlo (kMC) simulations from which nitrogen adsorption isotherms at 77 K could be obtained. The numerically generated isotherms show an excellent agreement with experimental data for the TPB-DMTP-COF monolith within the high-pressure region of the adsorption isotherms, providing complementary data to the GCMC-calculated isotherms and demonstrating the applicability of lattice gas models in capturing the inter-particle mesoporosity of COF monoliths. Collectively, these results suggest that the hierarchical porosity of COF monoliths can be accurately described computationally across the micro and mesoporous range, enabling robust future predictions of adsorption characteristics.

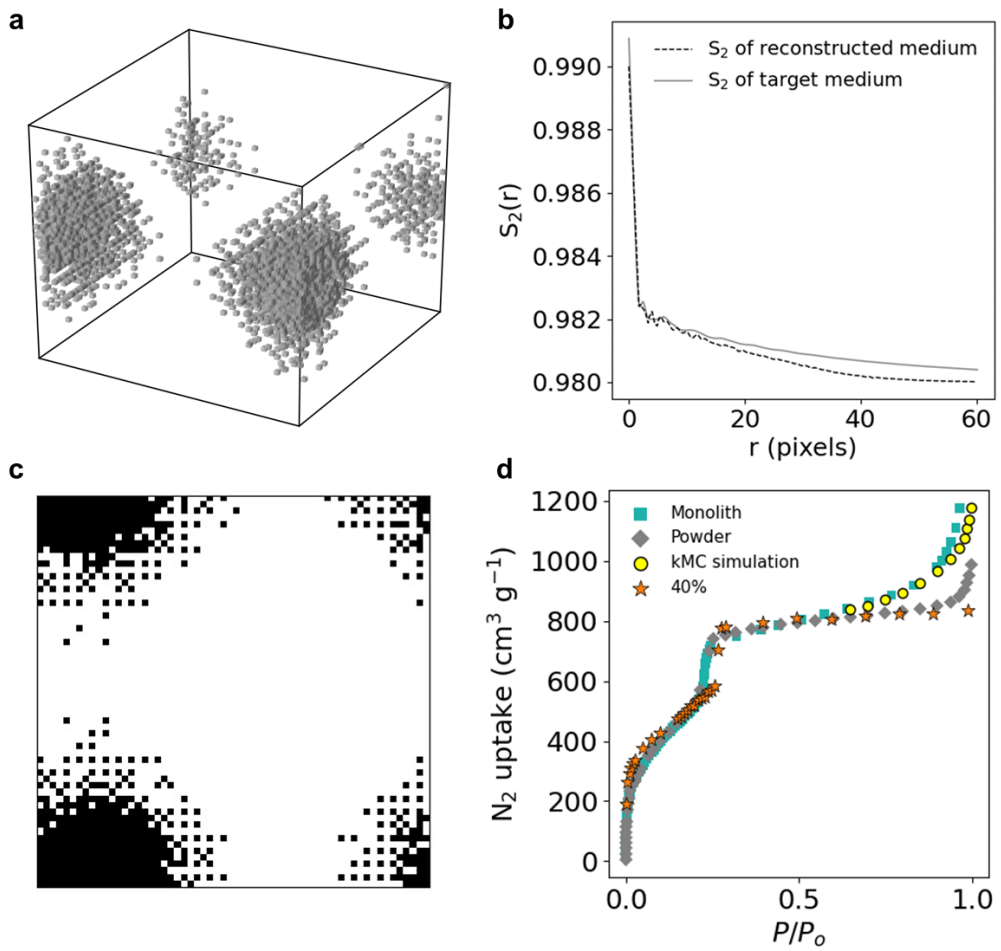

Figure 5 | Lattice gas model reconstruction and molecular simulations. (a) Reconstructed 3D realization of the TPB-DMTP-COF monolith defined on a **bcc** lattice with periodic boundaries; grey (white) voxels represent the solid (void) phase. **(b)** Comparison of $S_2(r)$ functions of target and reconstructed medium. The $S_2(r)$ function of the TPB-DMTP-COF monolith (target medium) is shown in grey and the $S_2(r)$ function of the reconstructed medium is shown in black (dashed line). **(c)** a 2D slice of the 3D realization showing all the possible sites occupied by the solid (in black) and void (in white) phases. The size of the system is 60 x 60 x 60 pixels for the 3D realization, and 60 x 60 pixels for the 2D slice. **(d)** Comparison of experimental adsorption isotherms to simulated adsorption isotherms of N_2 at 77 K. The experimental adsorption isotherms are represented by using the turquoise squares for the 3 bar h^{-1} $scCO_2$ activated 1.000 (v/v) monolith and grey diamonds for the powder. Yellow circles correspond to data points obtained by performing kMC simulations within the lattice gas model. Orange stars correspond to data points obtained by GCMC simulations taking into consideration a 40% slip between layers.

5. Gas adsorption characteristics of TPB-DMTP-COF monoliths

To demonstrate the utility of monolithic processing of COFs in gas storage applications, we performed pure-component adsorption studies on TPB-DMTP-COF powders and monoliths. Low-pressure isotherms collected at 298 K revealed good CO_2 (**Figures 6a** and **6d**) uptake for both powders and monoliths with modest to low CH_4 (**Figure 6a**) and N_2 (**Figure 6d**) uptake respectively for both systems. However, up to pressures of 1 bar, while higher CO_2 uptake was obtained for monoliths over powders, lower uptake for both CH_4 and N_2 were obtained for monoliths relative to powders. These results suggest that the presence of inter-particle mesopores in monoliths can not only

be used to improve final storage capacities for a single component but can be used to favourably or disfavourably influence final uptake characteristics of various components within a mixed feed.

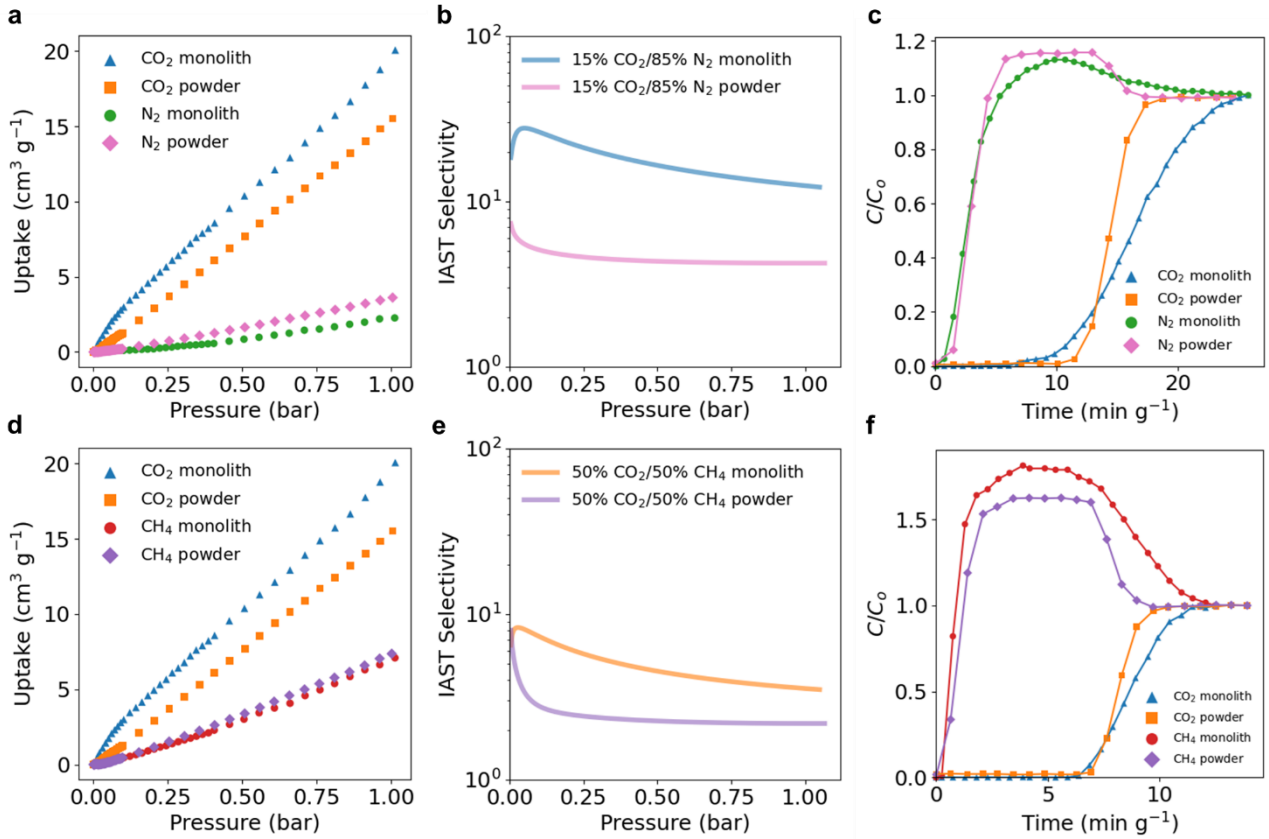

Figure 6 | Low-pressure adsorption isotherms, IAST selectivity, and breakthrough studies of TPB-DMTP-COF (3 bar h^{-1} scCO$_2$ activated 1.000 (v/v) monolith and powder control). **(a)** Low-pressure adsorption isotherms of CO_2 and N_2 at 298 K in TPB-DMTP-COF monolith – blue triangles for CO_2 and green circles for N_2 – and powder – orange squares for CO_2 and pink diamonds for N_2. **(b)** IAST selectivity as a function of pressure for a 15% CO_2/85% N_2 gas mixture for TPB-DMTP-COF monolith (blue) and powder (pink). **(c)** Breakthrough studies for a 15% CO_2/85% N_2 gas mixture for TPB-DMTP-COF monolith (CO_2 – blue triangles, N_2 – green circles) and powder (CO_2 – orange squares, N_2 – pink diamonds) at 298 K. (**d)** Low-pressure adsorption isotherms of CO_2 and CH_4 at 298 K in TPB-DMTP-COF monolith – blue triangles for CO_2 and red circles for CH_4 – and powder – orange squares for CO_2 and purple diamonds for CH_4. **(e)** IAST selectivity as a function of pressure for a 50% CO_2/50% CH_4 gas mixture for TPB-DMTP-COF monolith (orange) and powder (purple). **(f)** Breakthrough studies for a 50% CO_2/50% CH_4 gas mixture for TPB-DMTP-COF monolith (CO_2 – blue triangles, CH_4 – red circles) and powder (CO_2 – orange squares, CH_4 – purple diamonds) at 298 K.

To examine these characteristics within the context of chemical separations, we evaluated adsorption selectivities for industrially relevant compositions of CO_2, CH_4 and N_2 mixtures. From pure-component adsorption isotherms, and using the Ideal Absorbed Solution Theory (IAST), we calculated selectivities for 15% CO_2 / 85% N_2 (**Figure 6e**) and 50% CO_2 / 50% CH_4 (**Figure 6b**) (v/v) mixtures. At low pressures, the selectivity for CO_2 relative to other components was substantially improved, providing evidence that monolithic COF structuring can be used to provide separation enhancements relative to unstructured COF powders. To confirm this, we performed dynamic

breakthrough studies on TPB-DMTP-COF monoliths and powders using mixed gas feeds. For the 15% CO_2 / 85% N_2 mixture (**Figure 6f**), while a comparable separation was achieved for the monolith relative to the powder, with some additional evidence for axial dispersion observed, the total CO_2 uptake was found to be 13.4% higher for the monolith. For the 50% CO_2 / 50% CH_4 mixture (**Figure 6c**), a markedly sharper separation for the monolith was observed relative to the powder with an additional improvement in CO_2 capacity of 8.6% achieved. Collectively, these results not only demonstrate the utility of monolithic processing for adsorbent-based chemical storage and separation but afford additional degrees of freedom through which the properties of COFs can be systematically designed and tuned.

6. Conclusions

Using a simple and general processing workflow, we introduce methods for the preparation of hierarchically porous COF monoliths without the need for additional materials or processing components. We show that such processing methods are compatible with mechanically weak materials, and further afford degrees of design freedom in the control of both extrinsic and intrinsic porosity. These characteristics endow monolithic COFs with properties that are distinct from both powder and single-crystal analogues, which we accurately capture *in silico* using a lattice gas model. We envision that such computational approaches can be used in future to predict gas uptake properties for broad classes of monolithic mesoporous materials. The extrinsic porosity present in COF monoliths can further be leveraged to simultaneously increase and decrease the final uptake capacities for various gas constituents relative to powder benchmarks, which we make use of in demonstrating improved separation performance for industrially relevant gas compositions. We believe that this study not only opens up new possibilities for the practical applicability of COFs but provides a pathway forward for tuning sorbent-analyte interactions where changes to the underlying framework chemistry may not be possible or synthetically accessible.

7. Methods

Materials

Scandium(III)trifluoromethanesulfonate (98%) was purchased from Alfa Aesar, 1,3,5-tris(4-aminophenyl)benzene (93%) was purchased from TCI, 2,5-dimethoxybenzene-1,4-dicarboxaldehyde (97%) was purchased from Sigma-Aldrich, methanol (99.9%), acetonitrile (99.9+%), 1,3,5-trimethylbenzene (99%), 1,4-dioxane (99.5%), were purchased from Acros Organics. All chemicals were used as received without further purification.

Synthesis of TPB-DMTP-COFs

Monoliths

To a 50 mL centrifuge tube were added 1,3,5-tris(4-aminophenyl)benzene (140.60 mg, 400 µmol) and 2,5-dimethoxybenzene-1,4-dicarboxaldehyde (29.13 mg, 150 µmol). Solvent (16 mL) was then added and the mixture was sonicated briefly to a homogenous suspension. Scandium(III)trifluoromethanesulfonate[22] (12 mg, 24 µmol) was added, the tube was sealed, and the mixture was sonicated again for *ca.* 20 seconds. The mixture was then left to react for 30 minutes undisturbed. The sample was collected by centrifugation for 50 minutes, washed with three portions of solvent (40 mL each) and an additional portion of methanol (40 mL), and was solvent exchanged in methanol (40 mL) at 50 °C for 48 hours, with the solvent being replaced after 24 hours. The solvent was then decanted, and the sample was washed with methanol (40 mL), and left to dry at 20 °C for a further 24 hours, or dried using supercitical carbon dioxide. The sample was activated overnight at 120 °C under vacuum prior to characterization.

Powders

The TPB-DMTP-COF powder controls were synthesized using a previously reported procedure[14].

Characterization of TPB-DMTP-COF

Total scattering data was collected at beamline 11-ID-B of the Advanced Photon Source (APS), Argonne National Laboratory (ANL), IL, USA.[23] Monoliths were segmented into regions (rim, top, and bottom; **Figure S6**) and lightly ground before loading into 1.1 mm (O.D.) Kapton™ capillaries. High energy X-ray scattering data were recorded using a Perkin Elmer amorphous silicon-based area detector using an X-ray wavelength of 0.2115 Å at a sample-to-detector distance of *ca.* 180 mm – experimental geometry was calibrated using a CeO_2 diffraction standard. The images were calibrated and reduced to 1D diffraction data within GSAS-II.[24] The X-ray scattering measured for an empty Kapton™ capillary was used as the sample background. The data were background corrected in xPDFsuite,[25] and *G(r)* was calculated using data in the range 0.1 $Å^{-1} \leq Q \leq 23.1$ $Å^{-1}$. Full details and discussion on the total scattering data are included in the Supplementary Information, page S11. Scanning Electron Microscope (SEM) images were acquired using an FEI XL30 FEGSEM with an accelerating voltage of 5 kV. Samples were sputter coated with gold. Transmission Electron Microscopy was carried out on a FEI Tecnai F20 TEM operated at 200 kV, and images were acquired using a Gatan OneView camera.

Helium pycnometery was obtained using an AccuPyc 1330 Pycnometer from Micromeritics. This technique was used to estimate the particle density and the volume of both powders and monoliths by measuring the pressure change of helium in a calibrated volume. Each volume was recorded as an

average value of six consecutive runs. Prior to the analysis, all samples were activated overnight at 120 °C (vacuum) before measuring the mass.

Mercury Porosimetry was obtained up to a final pressure of 2,000 bar using an AutoPore IV 9500 instrument from Micromeritics. This technique was used to estimate the particle density of both powders and monoliths at atmospheric pressure. Prior to the analysis, all samples were activated overnight at 120 °C (vacuum) before measuring the mass, and then degassed in situ thoroughly before the mercury porosimetry.

Critical point dryer-CO_2 procedure. A SPI-DRY Critical Point Dryer - Jumbo modify with a manometer at the chamber was used to dry and activate the COF monoliths. First, the sample was transferred into a dialysis membrane (Spectra/P.1 MWCO 6-8 kD) and sealed. Then, the membrane was introduced into the critical point drying equipment. Then, it was immersed in subcritical (l) CO_2 at 283 K and 50 bar for half an hour. Then, the exchanged methanol was removed through a purge valve followed by flushing with fresh (l) CO_2. This process was repeated three times. Subsequently, the temperature was raised 5 K min^{-1} up to 313 K to exceed supercritical CO_2 point. Finally, under constant temperature (313 K), the chamber was vented at 8 bar h^{-1} or 3 bar h^{-1} to atmospheric pressure.

Gas Adsorption Measurements. Ultra-high-purity grade CH_4, N_2 and CO_2 were used for gas sorption experiments. Adsorption experiments (up to 1 bar) for different pure gases were performed on Micromeritics 3 Flex surface area and pore size analyzer. About 200 mg of activated samples were used for the measurements. A temperature-controlled bath was used to maintain a constant temperature in the bath through the duration of the experiment. Samples were degassed on a Micromeritics PrepStation instrument prior to the analysis.

Dynamic mixed gas breakthrough studies

In a typical experiment, *ca.* 0.3 g of pre-activated sample was placed in a quartz tube (Ø = 8 mm) to form a fixed bed held in place using quartz wool. For monolithic samples, individual monoliths were broken and sieved to reduce the particle diameter to *ca.* 2 mm to ensure good packing within the sample tube. Each sample was heated to 353 K under a dry helium flow to remove atmospheric contaminants. Upon cooling, the chosen gas mixture was passed over the packed bed with a total flow rate of 2 cm^3 min^{-1} at 298 K. The outlet gas concentration was continuously monitored using an Agilent 5975 MSD mass spectrometer (MS). Upon complete breakthrough and saturation of the

packed bed adsorbent, the gas mixture is switched off and dry helium was flowed over the solid. Heating was switch on and samples were heated to 353 K to aid regeneration.

To calculate the CO_2 uptake, initially, the gas mixture is passed through an empty reactor containing quartz wool at a flow rate of 2 cm^3 min^{-1} as a blank reference. The gas flow is constantly monitored using the MS. The CO_2 curve is integrated to calculate the area of the curve (A_{Ref}). Upon completion of a CO_2 breakthrough experiment with an adsorbent, the area of the CO_2 adsorption curve is also integrated (A_{Exp}). To calculate the total amount of CO_2 adsorbed, the following equation is used:

$$\text{Total } CO_2 \text{ Uptake} = (A_{Ref} - A_{Exp}) \times CO_2 \text{ flow } (cm^3\ min^{-1})$$

Molecular simulations

The adsorption isotherms of N_2 are simulated using the grand canonical Monte Carlo (GCMC) method as implemented in the RASPA simulation package[26]. The geometric properties have been calculated using Poreblazer[27, 28]. A more detailed description about the methodology and model parameters is given in the Supplementary Information, page S3.

Lattice gas model

First, the SAXS data collected was converted into a two-point correlation function $S_2(r)$- defined as the probability of two points separated a distance r apart, belong to the pore space of the medium - which was then used as a benchmark to create a 3D reconstruction of the TPB-DMTP-COF monolith. In order to model the trajectory of the system in the grand canonical ensemble, and to obtain the adsorption isotherms we employ kinetic Monte Carlo (kMC) simulations. A more detailed description about the reconstruction procedure and the kMC simulations is given in the Supplementary Information, page S8.

Mechanical properties calculation

Mechanical properties for the COFs present in the CURATED COF database are calculated using classical molecular mechanics via the 'constant strain approach' as implemented in the Forcite module of Materials Studio. Some structures in the CURATED COF database for which, either the mechanical or geometric property calculation failed, are excluded. The mechanical properties calculated include the shear modulus, bulk modulus, and young's modulus. A more detailed description of the methodology used is given in the Supplementary Information, page S10.

BET area calculation

BET areas have been calculated using a computational tool called BET surface identification (BETSI)

- a tool that makes an unambigious calculation of the BET area possible. More details about BETSI can be found in the Supplementary Information, page S23.

Data availability

The experimental dataset generated and/or analysed during the current study are available from the corresponding author on reasonable request.

Acknowledgements

M.E.C. acknowledges support of the HRH The Prince of Wales Commonwealth Scholarship and the Trinity Henry Barlow Scholarship (Honorary). N.R. acknowledges the support of the Cambridge International Scholarship and the Trinity Henry Barlow Scholarship (Honorary). The X-ray total scattering measurements and multivariate analysis was supported as part of GENESIS: A Next-Generation Synthesis Center, an Energy Frontier Research Center funded by the U.S. Department of Energy, Office of Science, Basic Energy Sciences under Award Number DE-SC0019212. This research used beamline 11-ID-B of the Advanced Photon Source, a US DOE Office of Science User Facility operated for the DOE Office of Science by Argonne National Laboratory under contract No. DE-AC02-06CH11357. D. F.-J. thanks the Royal Society for a University Research Fellowship. We thank the European Research Council (ERC) under the European Union's Horizon 2020 research and innovation programme (NanoMOFdeli), ERC-2016-COG 726380 and Innovate UK (104384). J.S.A. would like to acknowledge financial support from the MINECO (project PID2019-108453GB-C21).

Author contributions

M.E.C. and D.F.-J. designed the research. M.E.C. performed the material synthesis and characterization. M.E.C., D.G.M. and C.C. did the N_2 gas adsorption at 77K. D.G.M. and C.C. did the N_2, CO_2, CH_4 gas adsorption at 298K. D.G.M. did the dynamic mixed gas breakthrough analysis. N.P.M.C. carried out the SAXS and WAXS data collection. D.O.N. did the SAXS and WAXS data analysis. D.O.N and K.C. did the PDF-XRD data collection and analysis. G.D. carried out the TEM analysis. M.E.C. carried out the SEM analysis. N.R. and R.C. carried out the lattice gas modelling under the supervision of S.T. N.R. carried out the molecular simulations and mechanical property screens. J.A.M.I. did the $scCO_2$ drying and activation under the supervision of F.Z. J.S.A. carried out the mercury porosimetry. M.E.C., N.R., and D.F.-J. wrote the the manuscript with contributions from all authors.

Conflict of Interest

M.E.C. and D.F.-J. are inventors on International (WO) Patent Application No:

PCT/EP2020/075779 submitted by Cambridge Enterprise Limited that covers COF monoliths, as well as aspects of their use. D.F.-J. has a financial interest in the start-up company Immaterial Labs, which is seeking to commercialize metal–organic frameworks.

References

1. Sholl, D. S.; Lively, R. P., Seven chemical separations to change the world. *Nature* **2016,** *532* (7600), 435-7.
2. Schoedel, A.; Ji, Z.; Yaghi, O. M., The role of metal–organic frameworks in a carbon-neutral energy cycle. *Nature Energy* **2016,** *1* (4), 16034.
3. Diercks, C. S.; Yaghi, O. M., The atom, the molecule, and the covalent organic framework. *Science* **2017,** *355* (6328), eaal1585.
4. Slater, A. G.; Cooper, A. I., Function-led design of new porous materials. *Science* **2015,** *348* (6238), aaa8075.
5. Huang, N.; Wang, P.; Jiang, D., Covalent organic frameworks: a materials platform for structural and functional designs. *Nature Reviews Materials* **2016,** *1* (10), 16068.
6. Sick, T.; Rotter, J. M.; Reuter, S.; Kandambeth, S.; Bach, N. N.; Döblinger, M.; Merz, J.; Clark, T.; Marder, T. B.; Bein, T.; Medina, D. D., Switching on and off Interlayer Correlations and Porosity in 2D Covalent Organic Frameworks. *Journal of the American Chemical Society* **2019,** *141* (32), 12570-12581.
7. Feriante, C. H.; Jhulki, S.; Evans, A. M.; Dasari, R. R.; Slicker, K.; Dichtel, W. R.; Marder, S. R., Rapid Synthesis of High Surface Area Imine-Linked 2D Covalent Organic Frameworks by Avoiding Pore Collapse During Isolation. *Advanced Materials* **2020,** *32* (2), 1905776.
8. Zhu, D.; Verduzco, R., Ultralow Surface Tension Solvents Enable Facile COF Activation with Reduced Pore Collapse. *Acs Appl Mater Inter* **2020,** *12* (29), 33121-33127.
9. Zhou, W.; Wu, H.; Yildirim, T., Structural stability and elastic properties of prototypical covalent organic frameworks. *Chem Phys Lett* **2010,** *499* (1), 103-107.
10. Sun, J.; Iakunkov, A.; Baburin, I. A.; Joseph, B.; Palermo, V.; Talyzin, A. V., Covalent Organic Framework (COF-1) under High Pressure. *Angewandte Chemie International Edition* **2020,** *59* (3), 1087-1092.
11. Du, Y.; Calabro, D.; Wooler, B.; Li, Q.; Cundy, S.; Kamakoti, P.; Colmyer, D.; Mao, K.; Ravikovitch, P., Kinetic and Mechanistic Study of COF-1 Phase Change from a Staggered to Eclipsed Model upon Partial Removal of Mesitylene. *The Journal of Physical Chemistry C* **2014,** *118* (1), 399-407.
12. Uribe-romo, F. J.; Vazquez-molina, D.; Harper, J. K., Mechanically shaped 2-dimensional covalent organic frameworks. Google Patents: 2019.
13. Peyman Z. Moghadam, S. M. J. R., Aurelia Li, Chun-Man Chow, Jelle Wieme, Noushin Moharrami, Marta-Aragones-Anglada, Gareth Conduit, Diego A. Gomez-Gualdron, Veronique Van Speybroeck, and David Fairen-Jimenez, Structure-Mechanical Stability Relations of Metal-Organic Frameworks via Machine Learning. *Matter* **2019,** *1*, 219-234.
14. Xu, H.; Gao, J.; Jiang, D., Stable, crystalline, porous, covalent organic frameworks as a platform for chiral organocatalysts. *Nature Chemistry* **2015,** *7* (11), 905-912.
15. Ongari, D.; Yakutovich, A. V.; Talirz, L.; Smit, B., Building a Consistent and Reproducible Database for Adsorption Evaluation in Covalent–Organic Frameworks. *ACS Central Science* **2019,** *5* (10), 1663-1675.
16. Howarth, A. J.; Liu, Y.; Li, P.; Li, Z.; Wang, T. C.; Hupp, J. T.; Farha, O. K., Chemical, thermal and mechanical stabilities of metal–organic frameworks. *Nature Reviews Materials* **2016,** *1* (3), 15018.
17. Tian, T.; Zeng, Z. X.; Vulpe, D.; Casco, M. E.; Divitini, G.; Midgley, P. A.; Silvestre-Albero, J.; Tan, J. C.; Moghadam, P. Z.; Fairen-Jimenez, D., A sol-gel monolithic metal-organic framework with enhanced methane uptake. *Nat Mater* **2018,** *17* (2), 174-+.

18. Connolly, B. M.; Aragones-Anglada, M.; Gandara-Loe, J.; Danaf, N. A.; Lamb, D. C.; Mehta, J. P.; Vulpe, D.; Wuttke, S.; Silvestre-Albero, J.; Moghadam, P. Z.; Wheatley, A. E. H.; Fairen-Jimenez, D., Tuning porosity in macroscopic monolithic metal-organic frameworks for exceptional natural gas storage. *Nature Communications* **2019,** *10*.
19. Connolly, B. M.; Madden, D. G.; Wheatley, A. E. H.; Fairen-Jimenez, D., Shaping the Future of Fuel: Monolithic Metal–Organic Frameworks for High-Density Gas Storage. *Journal of the American Chemical Society* **2020,** *142* (19), 8541-8549.
20. Chapman, K. W.; Halder, G. J.; Chupas, P. J., Pressure-Induced Amorphization and Porosity Modification in a Metal−Organic Framework. *Journal of the American Chemical Society* **2009,** *131* (48), 17546-17547.
21. Osterrieth, Johannes; Rampersad, James; Madden, David G.; Rampal, Nakul; Skoric, Luka; Connolly, Bethany; et al.: How Reproducible Are Surface Areas Calculated from the BET Equation? *ChemRxiv. Preprint* **2021**. https://doi.org/10.26434/chemrxiv.14291644.v1
22. Matsumoto, M.; Dasari, R. R.; Ji, W.; Feriante, C. H.; Parker, T. C.; Marder, S. R.; Dichtel, W. R., Rapid, Low Temperature Formation of Imine-Linked Covalent Organic Frameworks Catalyzed by Metal Triflates. *Journal of the American Chemical Society* **2017,** *139* (14), 4999-5002.
23. Chupas, P. J.; Chapman, K. W.; Lee, P. L., Applications of an amorphous silicon-based area detector for high-resolution, high-sensitivity and fast time-resolved pair distribution function measurements. *J Appl Crystallogr* **2007,** *40*, 463-470.
24. Toby, B. H.; Von Dreele, R. B., GSAS-II: the genesis of a modern open-source all purpose crystallography software package. *J Appl Crystallogr* **2013,** *46*, 544-549.
25. Yang, X.; Juhas, P.; Farrow, C.; Billinge, S., xPDFsuite: an end-to-end software solution for high throughput pair distribution function transformation, visualization and analysis. *arXiv: Materials Science* **2014**.
26. Dubbeldam, D.; Calero, S.; Ellis, D. E.; Snurr, R. Q., RASPA: molecular simulation software for adsorption and diffusion in flexible nanoporous materials. *Mol Simulat* **2016,** *42* (2), 81-101.
27. Sarkisov, L.; Harrison, A., Computational structure characterisation tools in application to ordered and disordered porous materials. *Mol Simulat* **2011,** *37* (15), 1248-1257.
28. Sarkisov, L.; Bueno-Perez, R.; Sutharson, M.; Fairen-Jimenez, D., Materials Informatics with PoreBlazer v4.0 and the CSD MOF Database. *Chemistry of Materials* **2020,** *32* (23), 9849-9867.